Backstepping Control of the Plasma Current Profile in the DIII-D Tokamak

Mark D. Boyer, Justin Barton, Eugenio Schuster, Tim C. Luce, John R. Ferron, Michael L. Walker, David A. Humphreys, Ben G. Penaflor and Robert D. Johnson

***Abstract*— Control of the spatial profile of plasma current in tokamak plasmas has been demonstrated to be a key condition for achieving advanced scenarios with improved confinement and possible steady-state operation. The dynamics of the current profile are nonlinear and coupled with several other plasma parameters, motivating the design of model-based controllers that can account for these complexities. In this work, we consider a control-oriented model of the current profile evolution in DIII-D and the problem of regulating the current profile around a desired feed-forward trajectory. In open-loop, the response of the system to disturbances and perturbed initial conditions may be undesirable. To improve the performance of the system, the PDE model is discretized in space using a finite difference method and a backstepping design is applied to obtain a discrete transformation from the original system into an asymptotically stable target system with desirable properties. Through a nonlinear transformation, the resulting boundary control law utilizes the total plasma current, total power, and line averaged density as actuators. A Simserver simulation study is done to test the controller's performance and its implementation in the DIII-D plasma control system. Finally, experimental results showing the ability of the controller to reject input disturbances and perturbations in initial conditions are presented.**

I. Introduction

Nuclear fusion is the process by which two light nuclei fuse together to form a heavier nucleus, and is accompanied by a conversion of mass into energy. Extremely high temperatures are needed in order for fusion reactions to occur frequently enough to make a fusion reactor useful as a source of energy. At these temperatures, the deuterium/tritium fuel mixture becomes a plasma. One of the most promising devices for confining and controlling this fusion plasma is the tokamak, which uses helical magnetic fields to trap the fuel particles. The ITER tokamak is the next experimental step for fusion research, and will attempt to prove the technical feasibility of a commercial nuclear fusion power plant. However, several challenging control problems remain.

One such challenge is to operate the tokamak with sufficiently long plasma discharges. A purely inductive plasma current cannot be sustained for extended periods of time and steady-state operation will require the plasma current to be primarily generated by non-inductive means. In a tokamak reactor, setting up a suitable toroidal current profile plays an important part in enabling high fusion gain and non-inductive sustainment of plasma current for steady-state operation [1].

This work was supported in part by the National Science Foundation CAREER Award program (ECCS-0645086) and the U.S. Department of Energy (DE-FG02-09ER55064, DE-FC02-04ER54698). M.D. Boyer (m.dan.boyer@lehigh.edu), J. Barton, and E. Schuster are with the Department of Mechanical Engineering and Mechanics, Lehigh University, Bethlehem, PA 18015, USA. T.C. Luce, J.R. Ferron, M.L. Walker, D.A. Humphreys, B.G. Penaflor, and R.D. Johnson are with General Atomics, San Diego, CA 92121, USA.

Progress towards current profile control at the JET tokamak can be found in [2], [3], [4] and profile control at Tore Supra and JT-60U tokamaks is discussed in [5], [6], [7]. The approach to current profile control taken at the DIII-D tokamak is to attempt to create the desired profile during the plasma current ramp-up and early flattop phases of the tokamak discharge and maintain this target profile during the rest of the discharge. The current profile evolution is related to the evolution of the poloidal magnetic flux, which can be modeled in normalized cylindrical coordinates by a parabolic partial differential equation (PDE) referred to as the magnetic diffusion equation. The poloidal flux profile is related to the safety factor q, which is the ratio of the number of times a magnetic field line goes toroidally around the tokamak to the number of times it goes around poloidally. Non-model-based active control of the evolution of the safety factor at the magnetic axis, $q(0)$, and the minimum safety factor q_{min} during the initial part of the plasma discharge has been tested at DIII-D [8]. The controller utilized either electron cyclotron heating (ECH) or neutral beam injection (NBI) equal to a feedforward value plus a term proportional to the error in q. Limitations, such as oscillations and instability under certain operating conditions, along with the complexity and nonlinearity of the system, motivate the design of a model-based controller that takes into account the dynamics of the q profile in response to the available actuators.

A control-oriented model of the current profile evolution in DIII-D was developed in [9]. Self-generated, non-inductive current sources were neglected in the model derivation, making the model appropriate for the inductively driven ramp-up and early flat-top phase of discharges or for L-mode (low confinement) discharges, which typically have a small fraction of self-generated non-inductive current. The dynamics of the current profile evolution can be controlled using three available actuators: total plasma current, non-inductive power, and average plasma density. Nonlinear combinations of these actuators enter the magnetic diffusion equation in the form of interior, boundary, and diffusivity control terms. Since the actuators are physically constrained in magnitude and rate of change, experiments have shown that some of the desired current profiles may not be achievable for all arbitrary initial conditions. Therefore, the objective becomes to minimize the profile error during the initial part of the discharge, which can be treated as a finite-time constrained optimal control problem for a nonlinear PDE system. Using this model, optimal open-loop (feed-forward) control algorithms were designed based on nonlinear programming [10] and extremum seeking [11] approaches. Since these optimal control inputs are computed off-line, they cannot be

modified in real-time to account for external disturbances, changes in the initial conditions, or model uncertainty. To achieve desired performance and robustness properties, it is necessary to close the loop with a feedback control law. A robust control approach to the problem considering the time-varying parts of the model as uncertainty, is proposed in [12] using all three types of actuation. In this work, we note the strong influence of the boundary control term on the system and seek a boundary feedback control law. This approach avoids the need to neglect any nonlinear terms or time-varying model terms and can be extended in the future to utilize the interior actuators. The PDE describing the current profile evolution is discretized in space using a finite difference method and a backstepping design is applied to obtain a discrete transformation from the original system into an asymptotically stable target system. This backstepping technique has been applied to other fusion systems, specifically the problem of kinetic profile control, in our work [13], [14], and [15]. Through a nonlinear transformation of the boundary control law, we obtain a feedback control law for the plasma current, non-inductive power, and line averaged density which is used to complement the feedforward control trajectories computed off-line. Numerical simulations show that improved performance is achieved through the use of this control scheme and the results are confirmed in an experiment on DIII-D.

The paper is organized as follows, In Section II a PDE model for the current profile evolution is introduced. The control objective is discussed in Section III. In Section IV, a backstepping feedback control law is presented and the control law is studied in simulations in Section V. Experimental results are presented in Section VI. Finally, conclusions and future work are stated in Section VII.

II. Current Profile Evolution Model

Let ρ be an arbitrary coordinate indexing the magnetic surfaces within the tokamak plasma. Any quantity constant on each surface could be chosen as the indexing variable. Here we choose the mean geometric radius of the magnetic surface as the variable ρ, i.e., $\pi B_{\phi,0}\rho^2 = \Phi$, where Φ is the toroidal magnetic flux and $B_{\phi,0}$ is the reference magnetic field at the geometric major radius R_0 of the tokamak. We normalize the quantity by ρ_b, the minor radius of the last closed magnetic surface, to obtain $\hat{\rho} = \rho/\rho_b$. The poloidal magnetic flux evolution along this normalized radial coordinate is given by the magnetic diffusion equation [9]

$$\frac{\partial \psi}{\partial t} = \frac{\eta(T_e)}{\mu_0 \rho_b^2 \hat{F}^2}\frac{1}{\hat{\rho}}\frac{\partial}{\partial \hat{\rho}}\left(\hat{\rho}\hat{F}\hat{G}\hat{H}\frac{\partial \psi}{\partial \hat{\rho}}\right) + R_0 \hat{H}\eta(T_e)\frac{<\bar{j}_{NI}\cdot\bar{B}>}{B_{\phi,0}} \tag{1}$$

where ψ is the poloidal magnetic flux, t is time, η is the plasma resistivity, which is dependent on the electron temperature, T_e, μ_0 is the vacuum permeability, $\bar{j}_{NI}$ is the non-inductive current density (from NBI, ECH, etc.), $\bar{B}$ is the magnetic field, and $<>$ denotes the flux-surface average of a quantity. $\hat{F}$, $\hat{G}$, and $\hat{H}$ are spatially varying geometric factors of the DIII-D tokamak and are described in [9]. The boundary conditions are given by

$$\left.\frac{\partial \psi}{\partial \hat{\rho}}\right|_{\hat{\rho}=0} = 0 \qquad \left.\frac{\partial \psi}{\partial \hat{\rho}}\right|_{\hat{\rho}=1} = -\frac{\mu_0}{2\pi}\frac{R_0}{\hat{G}\Big|_{\hat{\rho}=1}\hat{H}\Big|_{\hat{\rho}=1}} I(t)$$

where $I(t)$ denotes the total plasma current.

From experimental observations at DIII-D, simplified scenario-oriented models for the electron temperature, non-inductive current density, and plasma resistivity were identified [9]. Using these models allows us to write the magnetic diffusion equation (1) as

$$\frac{\partial \psi}{\partial t} = f_1(\hat{\rho})u_1(t)\frac{1}{\hat{\rho}}\frac{\partial}{\partial \hat{\rho}}\left(\hat{\rho}f_4(\hat{\rho})\frac{\partial \psi}{\partial \hat{\rho}}\right) + f_2(\hat{\rho})u_2(t) \tag{2}$$

with boundary conditions

$$\left.\frac{\partial \psi}{\partial \hat{\rho}}\right|_{\hat{\rho}=0} = 0 \qquad \left.\frac{\partial \psi}{\partial \hat{\rho}}\right|_{\hat{\rho}=1} = -k_3 u_3(t)$$

where $f_1(\hat{\rho})$, $f_2(\hat{\rho})$, and $f_4(\hat{\rho})$ are functions of $\hat{\rho}$, k_3 is a constant, and

$$u_1(t) = \left(\frac{\bar{n}(t)}{I(t)\sqrt{P_{tot}(t)}}\right)^{3/2} \quad u_2(t) = \frac{\sqrt{P_{tot}(t)}}{I(t)} \quad u_3(t) = I(t)$$

We consider $I(t)$, the total plasma current, $P_{tot}(t)$ the total non-inductive power (NBI), and $\bar{n}(t)$, the line-averaged plasma density, as actuators. Note that the waveforms generated by the controller proposed in this work represent references to be sent to existing controllers for the respective quantities.

The safety factor $q(\rho,t) = -d\Phi/d\Psi(\rho,t)$ can be used to specify the toroidal current density. Noting the constant relationship between ρ and Φ, i.e., $\pi B_{\phi,0}\rho^2 = \Phi$, and the definition of ρ_b, the safety factor can be written as

$$q(\hat{\rho},t) = -\frac{B_{\phi,0}\rho_b^2\hat{\rho}}{\partial\psi/\partial\hat{\rho}}$$

As the safety factor q inversely depends on the spatial derivative of the poloidal flux, we define

$$\theta(\hat{\rho},t) = \frac{\partial \psi}{\partial \hat{\rho}}(\hat{\rho},t) \tag{3}$$

and take this quantity as the to-be-controlled variable. To obtain a PDE for $\theta(\hat{\rho},t)$, we expand (2) using the chain rule, and insert (3) to obtain

$$\frac{\partial \psi}{\partial t} = f_1 u_1 \frac{1}{\hat{\rho}}\left[\hat{\rho}\theta f_4' + f_4\theta + \hat{\rho}f_4\theta'\right] + f_2 u_2 \tag{4}$$

where $(\cdot)' = \partial/\partial\hat{\rho}$ and the dependencies on time and space have been dropped to simplify the representation. By differentiating (4) with respect to $\hat{\rho}$, the PDE governing the evolution of $\theta(\hat{\rho},t)$ is found to be

$$\frac{\partial \theta}{\partial t} = h_0 u_1 \theta'' + h_1 u_1 \theta' + h_2 u_1 \theta + h_3 u_2 \tag{5}$$

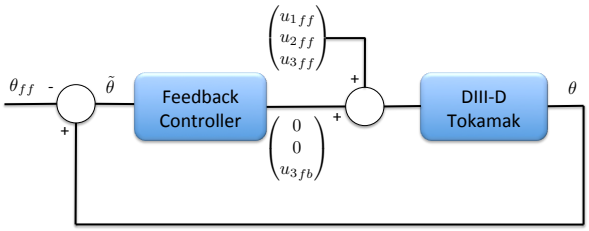

Fig. 1: Control scheme.

with boundary conditions:

$$\theta\Big|_{\hat{\rho}=0} = 0 \qquad \theta\Big|_{\hat{\rho}=1} = -k_3 u_3(t) \tag{6}$$

where h_0, h_1, h_2, and h_3 are functions of $\hat{\rho}$.

III. Control Objective

Let $u_{ff}(t)$ represent a feedforward control trajectory and $\theta_{ff}(\hat{\rho},t)$ be the associated state trajectory for a nominal initial condition $\theta_{ff}(\hat{\rho},0)$. These variables satisfy

$$\frac{\partial \theta_{ff}}{\partial t} = h_0 u_{1_{ff}} \theta''_{ff} + h_1 u_{1_{ff}} \theta'_{ff} + h_2 u_{1_{ff}} \theta_{ff} + h_3 u_{2_{ff}} \tag{7}$$

$$\theta_{ff}\Big|_{\hat{\rho}=0} = 0 \qquad \theta_{ff}\Big|_{\hat{\rho}=1} = -k_3 u_{3_{ff}}(t) \tag{8}$$

Given errors in initial conditions or other perturbations, the actual state will be $\theta = \theta_{ff} + \tilde{\theta}$. In this work, we will consider the design of a feedback law for the boundary control term u_3. We can then write $u_3 = u_{3_{ff}} + u_{3_{fb}}$ and the PDE (5) can be written as

$$\begin{aligned} \frac{\partial \left(\theta_{ff} + \tilde{\theta}\right)}{\partial t} =& h_0 u_{1_{ff}} \left(\theta''_{ff} + \tilde{\theta}''\right) + h_1 u_{1_{ff}} \left(\theta'_{ff} + \tilde{\theta}'\right) \\ &+ h_2 u_{1_{ff}} \left(\theta_{ff} + \tilde{\theta}\right) + h_3 u_{2_{ff}} \end{aligned}$$

$$\left(\theta_{ff} + \tilde{\theta}\right)\Big|_{\hat{\rho}=0} = 0 \quad \left(\theta_{ff} + \tilde{\theta}\right)\Big|_{\hat{\rho}=1} = -k_3 \left(u_{3_{ff}} + u_{3_{fb}}\right)$$

Noting (7) and (8), these expressions can be reduced to

$$\frac{\partial \tilde{\theta}}{\partial t} = h_0 u_{1_{ff}} \tilde{\theta}'' + h_1 u_{1_{ff}} \tilde{\theta}' + h_2 u_{1_{ff}} \tilde{\theta} \tag{9}$$

$$\tilde{\theta}\Big|_{\hat{\rho}=0} = 0 \qquad \tilde{\theta}\Big|_{\hat{\rho}=1} = -k_3 u_{3_{fb}} \tag{10}$$

The control objective is to drive $\tilde{\theta}$ to zero through the use of the boundary feedback term $u_{3_{fb}}$. The control scheme is illustrated in Figure 1.

IV. Backstepping Boundary Controller

A backstepping technique is used to transform a discretized version of the original system of equations into an asymptotically stable target system. The technique is illustrated in Figure 2.

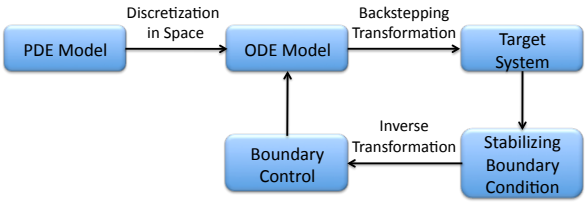

Fig. 2: Backstepping control technique.

By defining $h = \frac{1}{N}$, where N is an integer, and using the notation $x^i(t) = x(ih,t)$, the model (9) can be written as

$$\begin{aligned} \dot{\tilde{\theta}}^i =& h_0^i u_{1_{ff}} \frac{\tilde{\theta}^{i+1} - 2\tilde{\theta}^i + \tilde{\theta}^{i-1}}{h^2} + h_1^i u_{1_{ff}} \frac{\tilde{\theta}^{i+1} - \tilde{\theta}^{i-1}}{2h} \\ &+ h_2^i u_{1_{ff}} \tilde{\theta}^i \end{aligned} \tag{11}$$

with boundary conditions (10) written

$$\tilde{\theta}^0 = 0 \qquad \tilde{\theta}^N = -k_3 u_{3_{fb}} \tag{12}$$

Since the open loop system is stable, we choose the target system to be

$$\begin{aligned} \dot{\tilde{w}}^i =& h_0^i u_{1_{ff}} \frac{\tilde{w}^{i+1} - 2\tilde{w}^i + \tilde{w}^{i-1}}{h^2} + h_1^i u_{1_{ff}} \frac{\tilde{w}^{i+1} - \tilde{w}^{i-1}}{2h} \\ &+ h_2^i u_{1_{ff}} \tilde{w}^i - C_w^i u_{1_{ff}} \tilde{w}^i \end{aligned} \tag{13}$$

with boundary conditions written as

$$\tilde{w}^0 = 0 \qquad \tilde{w}^N = 0 \tag{14}$$

The design parameters $C_w^i > 0$ are chosen based on a trade-off between desired levels of robustness and performance and the physical actuator limits. Next, a backstepping transformation is sought in the form

$$\tilde{w}^i = \tilde{\theta}^i - \alpha^{i-1}\left(\tilde{\theta}^0, \ldots, \tilde{\theta}^{i-1}\right)$$

By subtracting (13) from (11), the expression $\dot{\alpha}^{i-1} = \dot{\tilde{\theta}}^i - \dot{\tilde{w}}^i$ is obtained in terms of $\alpha^{k-1} = \tilde{\theta}^k - \tilde{w}^k$, $k = i-1, i, i+1$. The resulting expression can then be solved for α^i to yield

$$\begin{aligned} \alpha^i = -\left[\frac{1}{\frac{h_0^i}{h^2} + \frac{h_1^i}{2h}}\right] \Bigg[& \left(\frac{-2h_0^i}{h^2} + h_2^i - C_w\right) \alpha^{i-1} \\ &+ \left(\frac{h_0^i}{h^2} - \frac{h_1^i}{2h}\right) \alpha^{i-2} - \frac{1}{u_{1_{ff}}} \dot{\alpha}^{i-1} + C_w \tilde{\theta}^i \Bigg] \end{aligned} \tag{15}$$

where $\alpha^0 = 0$ and $\dot{\alpha}^{i-1}$ is calculated as

$$\dot{\alpha}^{i-1} = \sum_{k=1}^{i-1} \frac{\partial \alpha^{i-1}}{\partial \tilde{\theta}^k} \dot{\tilde{\theta}}^k \tag{16}$$

Next, subtracting (14) from (12) and putting the resulting expression in terms of $\alpha^{k-1} = \tilde{\theta}^k - \tilde{w}^k$, $k = i-1, i, i+1$, the control law for $u_{3_{fb}}$ can be defined as

$$u_{3_{fb}} = -\frac{1}{k_3} \alpha^{N-1} \tag{17}$$

For any choice of grid size N, the control law (17) will be a time-invariant linear combination of $N-1$ measurements from the interior of the plasma. The coefficients of this linear

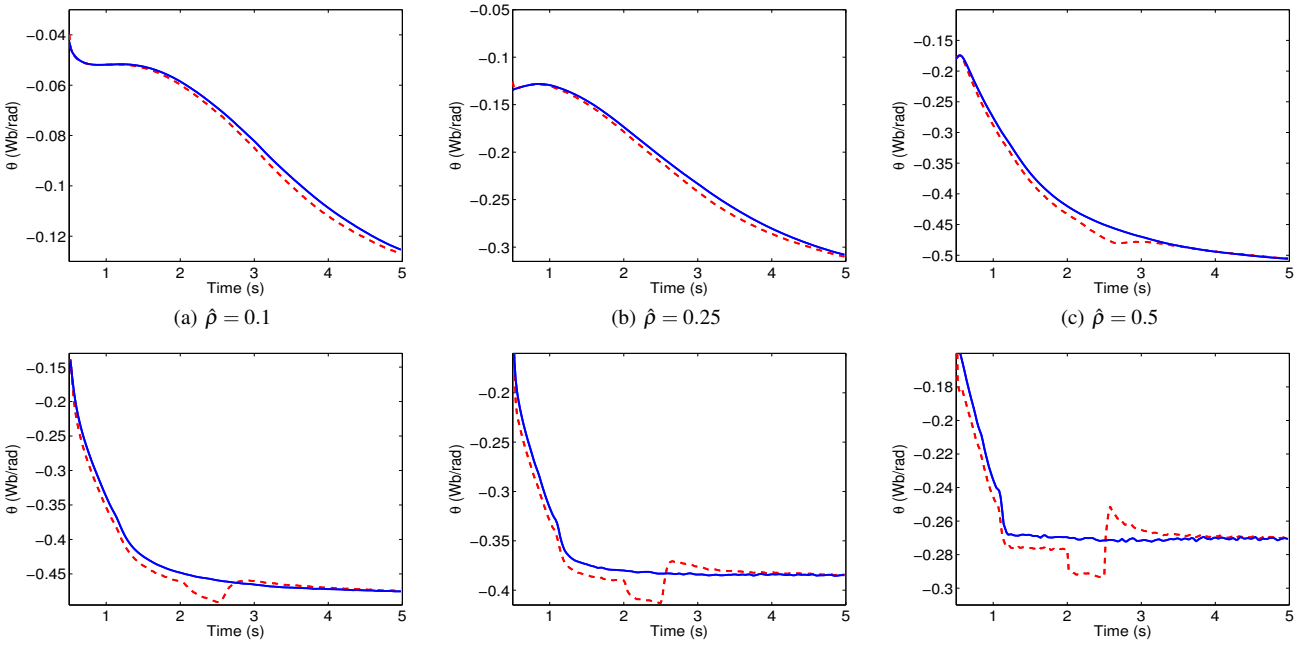

(a) $\hat{\rho} = 0.1$ (b) $\hat{\rho} = 0.25$ (c) $\hat{\rho} = 0.5$

(d) $\hat{\rho} = 0.65$ (e) $\hat{\rho} = 0.8$ (f) $\hat{\rho} = 0.95$

Fig. 3: Time trace of θ at various points comparing the feedforward simulation (blue-solid) and the closed loop, disturbed simulation (red-dashed).

combination can be calculated ahead of time for a given set of model parameters h_0, h_1, and h_2, and are independent of the feedforward inputs and trajectories.

The control law (17) gives the expression for the feedback part of u_3. The new value of u_3 is then used with the value u_2 and u_1 in the following nonlinear transformation to calculate the input requests I_p, P_{tot}, and $\bar{n}$:

$$I_p = u_3 \quad P_{tot} = u_3^2 u_{2_{ff}}^2 \quad \bar{n} = u_{1_{ff}}^{2/3} u_3^2 u_{2_{ff}} \tag{18}$$

These values are then sent as references to the respective dedicated controllers on the DIII-D device.

In order to facilitate the proof of stability, we write the target system as a matrix equation. By noting the boundary conditions (6), and defining $\mathbf{C_w}$ as a square diagonal matrix populated with the values of C_w^i for $1 \le i \le N-1$, the set of ODEs describing the target system can then be expressed as

$$\dot{\beta}(t) = (M - \mathbf{C_w})\,\beta(t) u_{1_{ff}}(t) \tag{19}$$

where $\beta = [w_1, \ldots, w_{N-1}]^T \in \mathbb{R}^{N-2\times 1}$ is the value of $\tilde{w}^i$ at the interior nodes, and M is a system matrix.

Taking $V = \frac{1}{2}\beta^T \Gamma \beta$ as a Lyapunov functional, where Γ is a positive definite matrix, we note that the first condition of Barbalat's lemma is satisfied, as $V > 0$ for $\beta \neq 0$. We can compute the time derivative as

$$\dot{V} = \beta^T \Gamma \dot{\beta} = \beta^T \Gamma (M - \mathbf{C_w})\, u_{1_{ff}}(t) \beta$$

Since $u_{1_{ff}}(t) > 0\, \forall t$ and Γ is positive definite, $(M - \mathbf{C_w})$ must be negative definite in order to ensure that $\dot{V}$ is negative semidefinite. For the model parameters used in this work, which are representative of a particular DIII-D discharge, and a grid size $N = 20$, we find that $max\{eig\{M\}\} = -6.7983 \times 10^{-16}$ (note that $u_{1_{ff}}(t) \sim 10^{15}$). As this is less than zero and $C_w^i \ge 0$ for $1 \le i \le N-1$, we can be sure that the matrix $(M - \mathbf{C_w})$ is negative definite and the second condition of Barbalat's lemma is satisfied. We can show that

$$\ddot{V} = 2u_{1_{ff}}^2(t) \beta^T \Gamma (M - \mathbf{C_w})(M - \mathbf{C_w})\beta + \dot{u}_{1_{ff}}(t) \beta^T \Gamma M \beta$$

which is bounded as long as $\dot{u}_{1_{ff}}(t)$ is bounded. Given this, the conditions of Barbalat's lemma are satisfied and we can be sure that $\dot{V} \to 0$ as $t \to \infty$, and, as a result, $\beta \to 0$. It can be seen from this analysis how the choice of $\mathbf{C_w}$ can adjust the speed of response of the system.

V. Simulation Results

A simulation study was done using a Simserver [16], which interfaces the DIII-D plasma control system with a Simulink implementation of the control oriented current profile evolution model. In this way, the controller performance and real-time implementation code could be tested before experimental testing. For the results presented here, as well as for the experimental results, the controller was designed using $C_w^i = 3.75 \times 10^{-16}$ for $1 \le i \le 5$ and $C_w^i = 7.5 \times 10^{-16}$ for $6 \le i \le N$ and with $N = 10$. In the simulation study, a particular set of feedforward inputs u_{ff} was used to generate a reference profile evolution θ_{ff}. The simulation was then run again, this time closing the loop with the feedback controller and adding input disturbances and perturbations in the initial conditions. An input disturbance of .1 MA in u_3 was added from $t = 0.5$s to $t = 2.5$s. The feedback controller was turned on from $t = 0.5$s to $t = 2.0$s to test disturbance rejection and switched off from $t = 2.0$s to $t = 2.5$s to allow the profile to drift away from the desired one under the

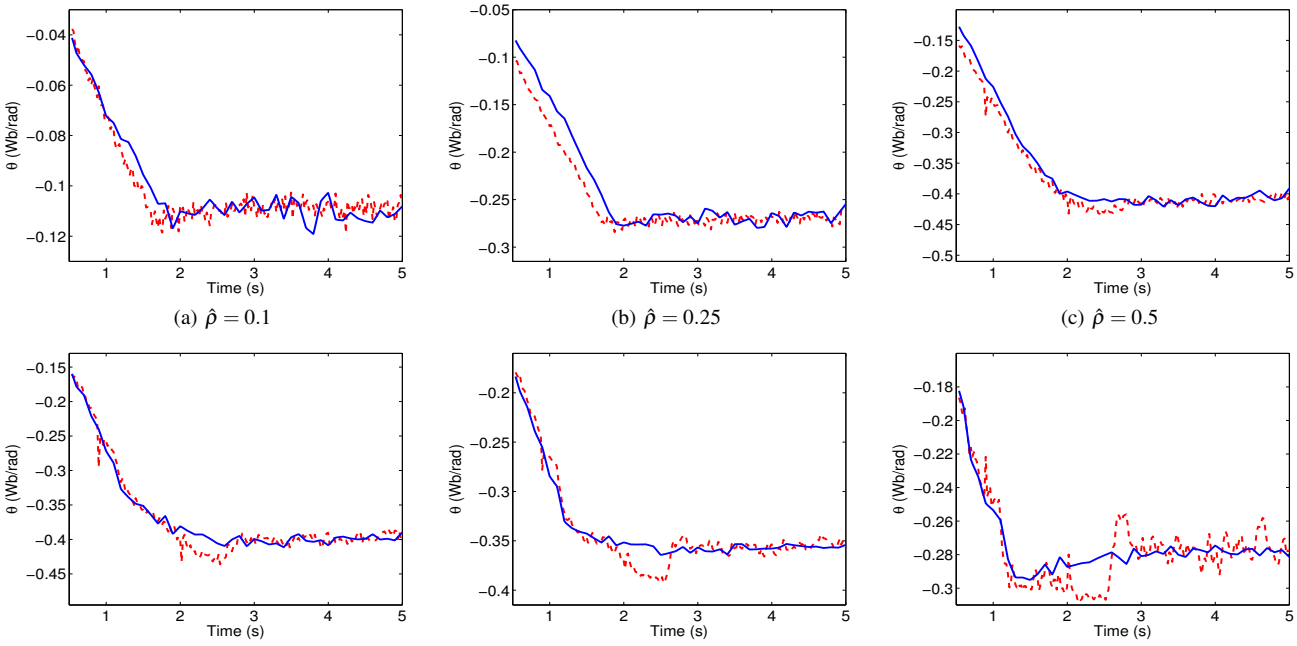

(a) $\hat{\rho} = 0.1$ (b) $\hat{\rho} = 0.25$ (c) $\hat{\rho} = 0.5$

(d) $\hat{\rho} = 0.65$ (e) $\hat{\rho} = 0.8$ (f) $\hat{\rho} = 0.95$

Fig. 4: Time trace of θ at various points comparing the reference shot 145477 (blue-solid) and the closed loop, disturbed shot 146454 (red-dashed).

influence of the input disturbance. Finally, at $t = 2.5$s the controller was turned back on and the input disturbance was removed to see if the controller could recover the desired profile despite the error caused by the drift.

Time traces of θ at several points along the profile are shown in Figure 3. The results of the closed loop simulation are compared with the reference generated in the feedforward simulation. A small steady state error is seen during the disturbance rejection phase of the simulation ($t = 0.5$s to $t = 2.0$s), which can be expected since there is no integral action in the controller. During the drift phase ($t = 2.0$s to $t = 2.5$s), the effect of the input disturbance can be seen diffusing in from the edge of the plasma over time. Finally, once the disturbance is removed and the controller is turned back on at $t = 2.5$s, the desired profile is quickly recovered.

VI. Experimental Results

In this section, we present experimental results showing the controller's performance on the DIII-D device. The same feedforward inputs used in the simulation were used to generate a reference shot, 145477. The resulting θ profile was then used as the target for the closed loop shot, 146454. For shot 146454, both the disturbances added to the feedforward inputs and the controller activation sequence were identical to those used in the closed loop simulation study. Time traces of θ at several points along the profile are given in Figure 4. The results of the closed loop shot 146454 are compared with the reference generated in the feedforward shot 145477. The controller appears to successfully reject the disturbance during the first phase ($t = 0.5$s to $t = 2.0$s) and the error caused by the disturbance without the presence of the feedback controller can clearly be seen moving in from the edge of the plasma during the drift phase ($t = 2.0$s to $t = 2.5$s). Finally, once the disturbance is removed and the controller is turned back on at $t = 2.5$s, the target values of θ are quickly recovered. By comparing Figures 3 and 4, it can be noted that the model makes a good prediction of the exterior points of the profile, but is less accurate at predicting the evolution of the interior points. The experimental results indicate that the controller design is robust to these modeling errors, however, performance improvement could be realized through model improvement. In Figure 5, the profiles achieved in the closed loop, disturbed shot 146454 are compared with the desired reference profiles obtained from shot 145477 at several times. Figure 5a shows that the controller has mostly rejected the disturbance and recovered the desired profile shortly before it is turned off at $t = 2.0$s. Figure 5b shows the error resulting from the disturbance after the uncontrolled drift phase ($t = 2.0s$ to $t = 2.5s$) and the successful recovery of the desired profile after the controller is turned back on for a short time is shown in Figure 5c. Finally, the actuator requests and achieved values are compared in Figure 6. It should be noted that while the total plasma current and total power requested by the proposed controller are reproduced quite well, the requests for density are often not achieved. This represents an additional input disturbance aside from the intentional one added to the feedforward input references. The controller seems to be robust to this added disturbance.

VII. Conclusions and Future Work

We have presented a current profile controller design based on the dynamic model for the evolution of the poloidal magnetic flux during the ramp-up phase of a DIII-D dis-

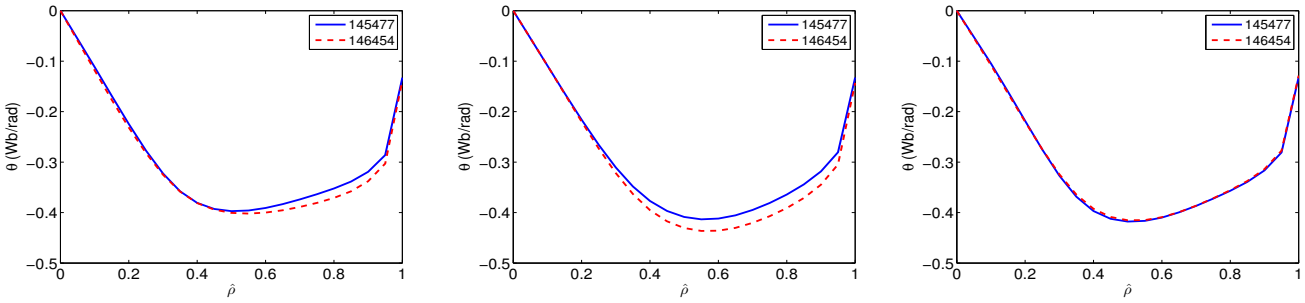

(a) $t = 1.98$s (feedback and disturbance on) (b) $t = 2.5$s (feedback off, disturbance on) (c) $t = 3.00$s (feedback on, disturbance off)

Fig. 5: Comparison of θ profiles at various times for reference shot 145477 (blue-solid) and the closed loop, disturbed shot 146454. Partial disturbance rejection is seen in (a), the effect of the uncontrolled disturbance can be noted in (b), and the recovery of the target profile after the disturbance is removed and the controller is turned back on can be observed in (c).

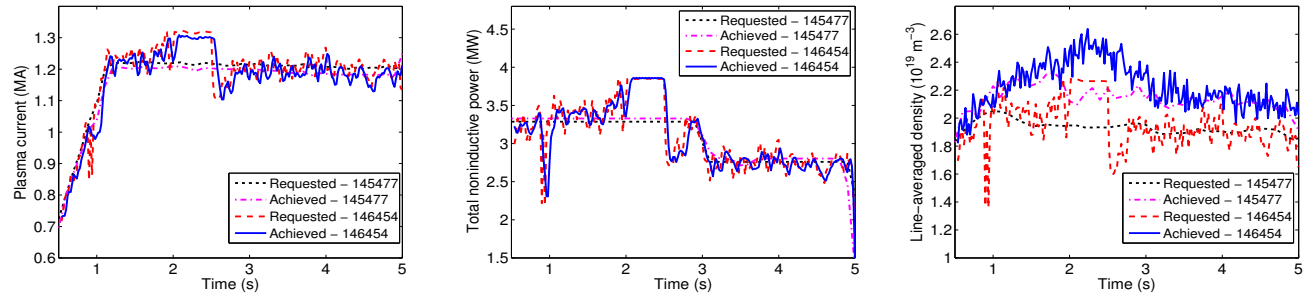

(a) Plasma current I_p (b) Total non-inductive power P_{tot} (c) Line averaged density $\bar{n}$

Fig. 6: Requested and achieved actuator values during feedforward shot 145477 and the closed loop, disturbed shot 146454.

charge. By employing a backstepping technique, a transformation was found from the spatially discretized system to an asymptotically stable target system with desirable properties. Through a nonlinear transformation, the resulting boundary feedback control law provides stabilizing reference values for the total plasma current, non-inductive power, and plasma density. A simulation study and experimental results show the performance of the controller when the initial conditions are perturbed and input is biased.

In the future, model improvements will be needed to extend the model to H-mode (high-confinement) discharges, for which the self-generated non-inductive current source neglected by the model used in this work becomes significant. Work will also be done to include feedback on the interior actuator terms u_1 and u_2. These extra degrees of freedom should improve performance. Additionally, integral action will be included in the control scheme to improve tracking and disturbance rejection.

REFERENCES

[1] M. Murakami, M. R. Wade, C. M. Greenfield, *et al.*, "Progress toward fully noninductive, high beta conditions in DIII-D," *Phys. of Plasmas*, vol. 13, no. 5, p. 056106, 2006.

[2] D. Moreau, D. Mazon, M. Ariola, , *et al.*, "A two-time-scale dynamic-model approach for magnetic and kinetic profile control in advanced tokamak scenarios on JET," *Nucl. Fusion*, vol. 48, no. 10, p. 106001, 2008.

[3] L. Laborde, D. Mazon, D. Moreau, *et al.*, "A model-based technique for integrated real-time profile control in the JET tokamak," *Plasma Phys. and Control. Fusion*, vol. 47, no. 1, pp. 155–183, 2005.

[4] D. Moreau, F. Crisanti, X. Litaudon, *et al.*, "Real-time control of the q -profile in JET for steady state advanced tokamak operation," *Nucl. Fusion*, vol. 43, no. 9, pp. 870–882, 2003.

[5] O. Barana, D. Mazon, L. Laborde, and F. Turco, "Feedback control of the lower hybrid power deposition profile on Tore Supra," *Plasma Phys. and Control. Fusion*, vol. 49, no. 7, pp. 947–967, 2007.

[6] T. Wijnands, D. V. Houtte, G. Martin, *et al.*, "Feedback control of the current profile on Tore Supra," *Nucl. Fusion*, vol. 37, no. 6, pp. 777–791, 1997.

[7] T. Suzuki, "Recent RF experiments and application of RF waves to real-time control of safety factor profile in JT-60U," *AIP Conference Proceedings*, vol. 787, pp. 279–286, 2005.

[8] J. Ferron, P. Gohil, C. Greenfield, *et al.*, "Feedback control of the safety factor profile evolution during formation of an advanced tokamak discharge," *Nucl. Fusion*, vol. 46, no. 10, pp. L13–L17, 2006.

[9] Y. Ou, T. Luce, E. Schuster, *et al.*, "Towards model-based current profile control at DIII-D," *Fusion Eng. and Design*, vol. 82, no. 5-14, pp. 1153–1160, 2007.

[10] C. Xu, Y. Ou, J. Dalessio, *et al.*, "Ramp-up-phase current-profile control of tokamak plasmas via nonlinear programming," *IEEE Trans. on Plasma Sci.*, vol. 38, no. 2, pp. 163–173, 2010.

[11] Y. Ou, C. Xu, E. Schuster, *et al.*, "Design and simulation of extremum-seeking open-loop optimal control of current profile in the DIII-D tokamak," *Plasma Phys. and Control. Fusion*, vol. 50, no. 11, p. 115001, 2008.

[12] J. Barton, W. Shi, M. D. Boyer, *et al.*, "Robust control of the current profile evolution during the ramp-up and early flat-top phases of the tokamak discharge.," in *Proc. of American Control Conf.*, 2012.

[13] M. D. Boyer and E. Schuster, "Backstepping control of density and energy profiles in a burning tokamak plasma," in *Proc. of Conf. on Decision and Control*, 2011.

[14] D. Boyer and E. Schuster, "Simultaneous control of effective atomic number and electron density in non-burning tokamak plasmas," in *Proc. of American Control Conf.*, 2010.

[15] E. Schuster and M. Krstić, "Control of a non-linear PDE system arising from non-burning tokamak plasma transport dynamics," *Int. J. of Control*, vol. 76, no. 11, pp. 1116–1124, 2003.

[16] M. Walker, J. R. Ferron, S. H. Hahn, *et al.*, "Advances in integrated plasma control on DIII-D," *Fusion Eng. and Design*, vol. 82, no. 5-14, pp. 1051–1057, 2007.